Neuroscience 329 (2016) 201–212

BLOCK DESIGN ENHANCES CLASSIFICATION OF 3D REACH TARGETS FROM ELECTROENCEPHALOGRAPHIC SIGNALS

RONEN SOSNIK,[a]* VIJAY ADITYA TADIPATRI,[b] AHMED H. TEWFIK[b] AND GIUSEPPE PELLIZZER[c,d]

[a] *Faculty of Electrical, Electronics and Communication Engineering, Holon Institute of Technology, Holon 5810201, Israel*

[b] *Electrical and Computer Engineering, The University of Texas, Austin, TX 78705, USA*

[c] *Brain Sciences Center, Veterans Affairs Health Care Center, Minneapolis, MN 55417, USA*

[d] *Department of Neuroscience, University of Minnesota, Minneapolis 55455, USA*

Abstract—To date, decoding accuracy of actual or imagined pointing movements to targets in 3D space from electroencephalographic (EEG) signals has remained modest. The reason may pertain to the fact that these movements activate essentially the same neural networks. In this study, we aimed at testing whether repetitive pointing movements to each of the targets promotes the development of segregated neural patterns, resulting in enhanced decoding accuracy. Six human subjects generated slow or fast repetitive pointing movements with their right dominant arm to one of five targets distributed in 3D space, followed by repetitive imagery of movements to the same target or to a different target. Nine naive subjects generated both repetitive and non-repetitive slow actual movements to each of the five targets to test the effect of block design on decoding accuracy. In order to assure that base line drift and low frequency motion artifacts do not contaminate the data, the data were high-pass filtered in 4–30 Hz, leaving out the delta and gamma band. For the repetitive trials, the model decoded target location with 81% accuracy, which is significantly higher than chance level. The average decoding rate of target location was only 30% for the non-repetitive trials, which is not significantly different than chance level. A subset of electrodes, mainly over the contralateral sensorimotor areas, was found to provide most of the discriminative features for all tested conditions. Time proximity between trained and tested blocks was found to enhance decoding accuracy of target location both by target non-specific and specific mechanisms. Our findings suggest that movement repetition promotes the development of distinct neural patterns, presumably by the formation of target-specific kinesthetic memory.

Key words: EEG, motor imagery, 3D reach movements, classification of targets, motor areas.

INTRODUCTION

Non-invasive electroencephalographic signals (EEG) have long been used to decode motor features. The decoding of movement onset or intention to move in self-paced reaching tasks is obtained generally using the 'Bereitschaftspotential' (BP), which is the negative potential deflection that precedes a movement (Deecke and Kornhuber, 2003), and/or from the event-related-desynchronization (ERD) associated with preparation and movement execution, such as the decrease in power from baseline of the alpha (~8–14 Hz) and beta bands (~15–30 Hz) (Tzagarakis et al., 2010). BP and ERD provide a signature deflection before the movement onset, making movement detection quite reliable (Kilner et al., 2004; Bai et al., 2011; Niazi et al., 2011). In addition, the lateralized difference in deflection between brain hemispheres provides decoding information of limb side in tasks that require the selection of either the left or right arm (Pfurtscheller et al., 2006; Huang et al., 2009; Nam et al., 2011).

The advent of high-quality multi-channel EEG recording systems and the significant advance in the field of machine learning enabled decoding more complex motion features, such as the direction of hand movement in real (Waldert et al., 2008) and imaginary conditions (Ofner and Muller-Putz, 2015). These decoding algorithms usually use classifiers like linear discriminant analysis (LDA) and support vector machine (SVM) on signal features to decode classes of movements, while other algorithms such as multivariate regression (MVR) are used to decode hand movement trajectories (Rickert et al., 2005). The signal features for decoding the direction of movement from one arm are most often extracted from the lowest frequency band (< 3 Hz, i.e., delta), although in some cases features from the alpha and beta bands also provided useful information (Brinkman et al., 2014). Studies that used 2D center-out paradigms to decode two classes (Lakany and Conway, 2007), three classes (Hammon et al., 2008) or four classes (Waldert et al., 2008; Robinson et al., 2013; Lew et al., 2014) of

*Corresponding author. Address: Holon Institute of Technology (HIT), 52 Golomb Street, Holon 5810201, Israel.
E-mail address: ronens@hit.ac.il (R. Sosnik).

Abbreviations: BCI, Brain–computer interface; BP, Bereitschafts-potential; CSP, Common Spatial Pattern; EEG, electroencephalogram; EMG, electromyogram; EOG, Electrooculography; ERD, event-related-desynchronization; FAM, fast actual movement; IBI, Inter Block Interval; ICA, Independent Component Analysis; ICs, independent components; IFM, imagery of fast movement; ISM, imagery of slow movement; JAD, joint approximate diagonalization; SAM, slow actual movement; SVM, support vector machine.

http://dx.doi.org/10.1016/j.neuroscience.2016.05.015

movements have reported success rates around 80%, 65% and 55%, respectively. When comparing the accuracy obtained in the different studies using the kappa coefficient – an index that allows performance comparison between studies with different number of categories – the decoding accuracy for three and four class 3D movements falls below 50%. Furthermore, in most studies targets are homogeneously distributed in the entire workspace, be it 2D (Wolpaw and McFarland, 2004; Robinson et al., 2013; Lew et al., 2014; Ofner and Muller-Putz, 2015) or 3D (Bradberry et al., 2010; Antelis et al., 2011), i.e., they are equally distributed around the starting position. This kind of target configuration may enhance decoding accuracy due to more distinct representations of target positions and movement profile.

In this work we aimed at testing whether block design enhances decoding of generated or imagined pointing movements to one of five targets positioned in the right side of the subject workspace using EEG data. While the classification of left hand, right hand, foot, and tongue imagined movements using EEG signal has been rather successful (Scherer et al., 2004; Wolpaw and McFarland, 2004), the discrimination of actual or imagined pointing movements to different targets with the same limb, on the other hand, is more challenging. This is due to the fact that these motor tasks activate essentially the same motor-related neural networks for all targets, thus, the discrimination between different actual or imagined movements has to rely more heavily on differences in temporal and spectral features of the neural activity rather than on differences in spatial activation patterns. In this study, we suggest that forming a distinct, target-specific neural activation pattern can be enhanced by segregating the internal representation of the different conditions (targets) and that this may be pursued by forming a strong recollection of each of the hand movements (muscle/kinesthetic memory) (Krakauer and Shadmehr, 2006). As kinesthetic memory involves consolidating a specific motor task into memory through repetition (Karni et al., 1995; Brashers-Krug et al., 1996; Shadmehr and Holcomb, 1997), a block design task was utilized in which each target is pointed at for several times consecutively.

EXPERIMENTAL PROCEDURES

Experimental paradigm

Fifteen healthy subjects (15 males, aged 25–46 years) gave informed consent and participated in the study, which was approved by the Wolfson Medical Center Helsinki committee. All subjects were right-handed, without any reported medical or psychological disease and/or medication and had normal or corrected to normal vision. The subjects sat 1.5 m in front of a motion sensing device (Microsoft Kinect) and were instructed not to move their head or talk throughout the entire experiment. The experimental design consisted of five targets; targets 1, 2 and 3 lay in the shoulder horizontal plane forming 45°, 67.5° and 90°, respectively, relative to a horizontal axis passing through the torso and shoulder, whereas targets 4 and 5 lay 45° below and above the shoulder sagittal plane, respectively, relative to a sagittal axis aligned with the shoulder (Fig. 1A).

Six subjects, denoted as Group I, practiced a block design task aimed at testing the model generalization to different motion velocities (slow and fast) and trial types (actual and imagery). Nine subjects, denoted as Group II, practiced both block design and non-block design aimed at testing the effect of the type of design on decoding accuracy. In order to avoid eye movements/blinks artifacts, the subjects were instructed to gaze at the aimed target (not to track their moving arm) and try to avoid eye blinks.

Group I

The subjects were informed that they should make, or imagine making repetitive pointing movements with their right dominant arm to one of the five targets distributed in the workspace and return to the home position ('H') in synchrony with an auditory cue (2-kHz and 1-kHz tone for a forward and backward movement, respectively).

The task consisted of nine blocks with one minute Inter Block Interval (IBI) (Fig. 1B). Each of the first five blocks (Block 1–5) comprised four sub blocks: slow actual movements (SAMs), imagery of slow movements (ISMs), fast actual movements (FAMs) and imagery of fast movements (IFMs), all aimed at the same target (T). The aimed target for block = {1, 2, 3, 4, 5) was T = {1, 2, 3, 4, 5}, respectively. Each of the last four blocks (Block 6–9) comprised two sub blocks: FAMs to target X followed by IFMs to target Y, wherein X = {1, 3, 2, 5} and Y = {5, 1, 4, 2} for block = {6, 7, 8, 9}, respectively. There was a ten seconds rest (R) between consecutive sub blocks.

Each slow sub block (actual or imagery) consisted of 15 trials whereas each fast sub block (actual or imagery) consisted of 24 fast trials, all aimed at the *same* target. Each slow (fast) trial comprised four epochs: 0.8 s (0.5 s) forward movement, 0.8 s (0.5 s) 'Pause at Target' rest, 0.8 s (0.5 s) backward movement and 0.8 s (0.5 s) 'Pause at Home' rest. Each slow or fast sub block lasted 48 s.

Group II

The task consisted of five blocks, all comprising SAMs with one minute IBI. All task characteristics (i.e., extrinsic cue, movement and sub block duration, IBI) remained as described above. Three blocks (denoted as 'non-repetitive' blocks) comprised non-repetitive, randomized movements, whereas two blocks (denoted as 'repetitive blocks' comprised repetitive movements.

'Non-repetitive' blocks. In order to test whether motor memory, evolving throughout the generation of repetitive movements, can provide a useful basis for improved decoding, data from repetitive blocks were contrasted with data from non-repetitive blocks. Hence, the subjects were instructed to perform a sequence of randomized movements to different targets rather than generating repetitive movements to one of the targets.

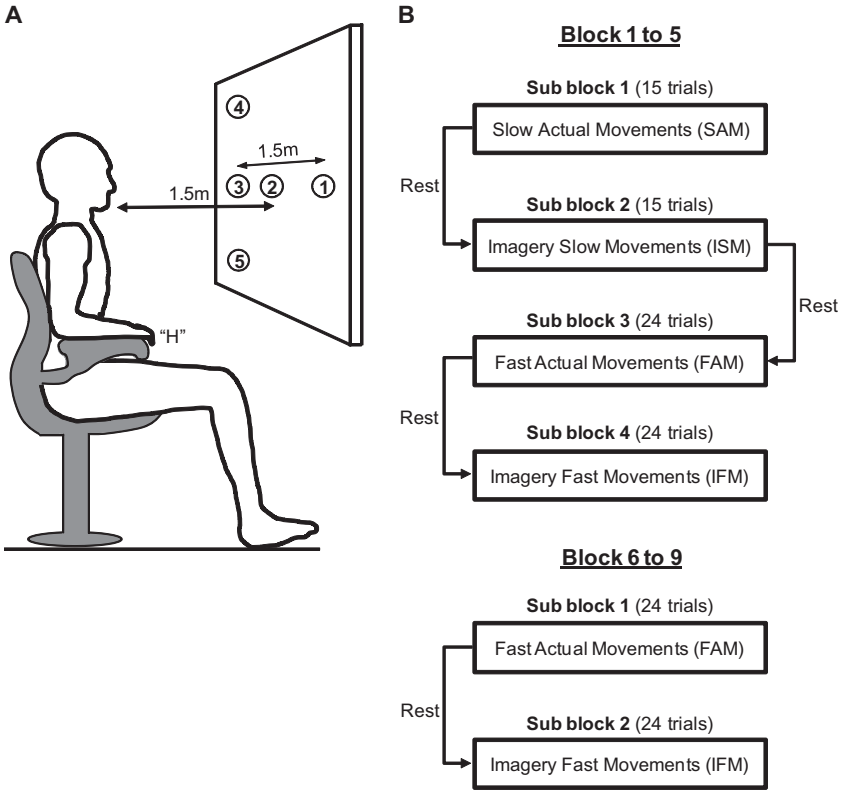

Fig. 1. Experimental setup – Group I. (A) Targets positions. Targets 1–3 lay in the shoulder plane forming 45°, 67.5° and 90°, respectively, relative to a horizontal axis passing through the torso and shoulder, whereas targets 4 and 5 lay 45° below and above the shoulder plane, relative to a sagittal axis aligned with the shoulder. The home position ('H') was a foam pad glued to the chair right armrest. (B) Experimental paradigm. For the first five blocks, a 'slow actual movement' sub block (comprising 15 trials) was followed by an 'imagery of slow movement' sub block (comprising 15 trials), a 'fast actual movement' sub block (comprising 24 trials) and an 'imagery of fast movement' sub block (comprising 24 trials), all aiming at the same target. For block 6–9, a 'fast actual movement' sub block (comprising 24 trials) to one of the targets was followed by an 'imagery of fast movement' sub block (comprising 24 trials) to a different target.

The targets and their order were set a priori, as asking a subject to select a different target for each movement may result in undesired consequences such as thinking at which target to point the following movement while the hand is still on the move, resulting in concurrent generation and planning of different movements or while the hand is resting in the 'Pause at Home' epoch, resulting in possible loss of a trigger cue. The subjects were informed of the upcoming sequence of movements at the beginning of each block. Specifically, each block comprised five identical sub blocks wherein a sub block comprised four identical sequences of SAMs to four different targets. The targets and their order were changed between the three blocks: {T2, T4, T5, T6}, {T1, T4, T3, T6} and {T1, T2, T5, T3} for block 1, 2 and 3, respectively.

'Repetitive' blocks. Each block comprised six sub blocks wherein each sub block comprised 15 repetitive movements to one of the targets (similar to the slow sub blocks of Group I). The order of the sub blocks was changed between the two blocks: {T1, T2, T4, T3, T6, T5} and {T1, T3, T6, T2, T4, T5} for the first block and second block, respectively. For all the five blocks, there was a ten-second rest between consecutive sub blocks.

In order to discard gel drying, attention loss or fatigue related artifacts, three subjects practiced the 'non-repetitive' blocks before the 'repetitive' blocks whereas the other three subjects practiced the 'repetitive' blocks before the 'non-repetitive' blocks. In order to test the generalization of hand trajectory decoding, a sixth target was added to the target configuration (results to be described elsewhere).

Data recording. We acquired parallel recorded electroencephalogram (EEG), electromyogram (EMG) and kinematic data in two computers connected by serial communication (RS232). The EEG and kinematic data were synchronized using timestamps. EEG signals were recorded from 62 active channels (with gel) and from one electrooculography (EOG) electrode that was attached inferiorly to the orbital fossa of the left eye (g. HIamp80, g.tec medical engineering GmbH, Schiedlberg, Austria). The EEG was referenced to the right ear lobe, amplified (gain: 20,000), filtered (Butterworth 0.5–100 Hz, 8th order) and sampled (A/D resolution: 24 bits, sampling rate: 1200 samples/s). The ground electrode was positioned over the Cz and impedance for all active electrodes was below 50 kΩ. We recorded surface EMG from the right arm biceps (BPMP150MW, BIOPAC systems, Inc., Goleta, CA,

USA). The EMG was amplified (gain: 2000), filtered (1–500 Hz), sampled (A/D resolution: 16 bits, sampling rate: 2000 samples/s), rectified and averaged (time window = 30 ms) in order to capture the "envelope" of the signal for later rejecting arm biceps artifacts (including mechanical artifacts) from the EEG signal using Independent Component Analysis (ICA) (denoizing). Next, the average rectified (AVR) EMG data was resampled at 1200 Hz to match the sampling rate of the EEG and EOG. Kinematic data were recorded from the right dominant hand, elbow and shoulder at 30 frames per second (FPS) using a 3D Microsoft Kinect camera system.

Computing trial length. A possible confound of the results is a difference in reach time to different targets and back to home position based on range-of-motion. In order to compute reach time (time difference between motion termination and initiation) to each of the targets, the kinematic data were first smoothed with a sixth order Butterworth filter, cut off frequency 8 Hz in order to remove the high frequency, small jerky movements caused by physiological tremor. Next, movement initiation and termination (both for forward and backward movements) were detected as the time point at which motion velocity firstly exceeded and fell below 10 cm/s, respectively, and movement time computed.

EEG data preprocessing. Data were preprocessed by 'FASTER' plug-in toolbox (Nolan et al., 2010) built on the open source EEGLAB (Delorme and Makeig, 2004), which allows automatic detection and correction of data artifacts in five aspects of the EEG data: channels, epochs, independent components (ICs), single-channel and single-epochs. First, the EEG data were passband filtered using an equiripple filter between 4–30 Hz in order to discard low-band (e.g., baseline drift and motion artifacts) and high-band (e.g., EMG) artifacts. The channels were analyzed for artifacts (a z score of $\geqslant 3$ for voltage amplitude (mV)) and any contaminated channels were interpolated. Next, the data were referenced to the average of all scalp electrodes and ICA was performed on the dataset. The resulting ICs were analyzed for artifacts and contaminated ICs were subtracted from the dataset. In order to extract the movement and imagery epochs, the data were cut around the auditory cue onset – from 0 ms to 800 ms, for the slow movements, and 0 to 500 ms, for the fast movements. The epochs were analyzed for artifacts and any contaminated epochs were removed from the dataset. Finally, the baseline (whole epoch mean) was removed from each epoch.

Feature extraction

Multi-class Common Spatial Pattern (CSP) filters were computed to extract discriminant information from multiple classes of EEG signals (Grosse-Wentrup and Buss, 2008). First, a covariance matrix was computed for each of the five target classes. Next, the five covariance matrices were used to compute a joint approximate diagonalization (JAD). It was shown that JAD of the EEG covariance matrices conditioned on class labels is an implementation of ICA, which is capable of separating the signal and the noise subspace under the stated assumptions and thus provides a suitable set of potential spatial filters (Grosse-Wentrup and Buss, 2008). Finally, the ICs that approximately maximized mutual information of class labels and extracted EEG components were computed. We then used four CSP filters as features, wherein each filter is the log of the weighted variance calculated on the multi-channel data. It should be noted that in contrast to two-classes CSP wherein the first and last columns of the weight matrix are the most important spatial patterns that explain the largest variance of one task and the smallest variance of the other, the first column of the weight matrix in the multi-class CSP is the spatial pattern that explains the largest variance of activation between all the conditions. In order to detect the electrodes whose activity is maximally different for different conditions, i.e., whose weight magnitude is high (irrespective of its sign), the absolute value of the first column of the weight matrix was computed for each of the training and testing datasets (see below) and averaged.

Feature classification

Group I – first five blocks. The first five blocks were used to assess the model specificity for a given target (class) and its generality within a class. For each target, trial type (actual/imagery) and speed (slow/fast) both movements (forward and backward) were pooled. In order to study the model specificity, a 5×5 cross-validation was performed; the data of each of the five classes of a given trial type and speed were divided into five parts (1–5), taking for each test four parts of the dataset for training and one part for testing. Hence, $5^5 = 3125$ different training and testing datasets were prepared, covering all possible combinations. For example, a single training dataset (out of 3125) of FAMs may comprise trials 1–20 of sub block 3, 7, 11, 15 and 19 (FAM-Targets 1, 2, 3, 4, and 5, respectively), and the corresponding test dataset comprising trials 21–24 of the respective sub block. Each of the training datasets was used to train a multi-class SVM (Crammer and Singer, 2001) with a radial basis function and classify the corresponding testing dataset. The votes for each class were counted and a confusion matrix computed. The abovementioned procedure was repeated for each of the two trial types and motion speeds. Finally, in order to test the model accuracy for decoding target location, irrespective of trial type, all the data were pooled across all conditions for each subject and used to train and test the model.

In order to study the generalization within a class, the model was trained and tested on different trial types and motion velocities. For example, in order to test whether the model generalized to a different motion speed to the same target, the model was trained on sub blocks 1, 5, 9, 13 and 17 (SAMs to targets 1, 2, 3, 4 and 5, respectively) and tested on sub blocks 3, 7, 11, 15 and 19 (FAMs to targets 1, 2, 3, 4 and 5, respectively). Fig. 3 summarizes the preprocessing steps and decoding steps.

Group I – last four blocks. The last four blocks were used to test for dependency of decoding accuracy on kinesthetic memory and time proximity between the training and testing blocks. The model was trained and tested on subsequent sub blocks; a sub block of FAMs to one of the targets (training data) was followed by a sub block of IFMs to a *different* target (testing data). For example, in order to test whether training on FAMs to target 1 (sub block 21) results in high decoding of IFMs to target 5 (sub block 22) simply due to their time proximity, the model was trained on sub blocks 7, 11, 15, 19 and 21 (FAMs to targets 2, 3, 4, 5 and 1, respectively) and tested on sub block 22 (IFMs to target 5). As was done for the first five blocks, all possible

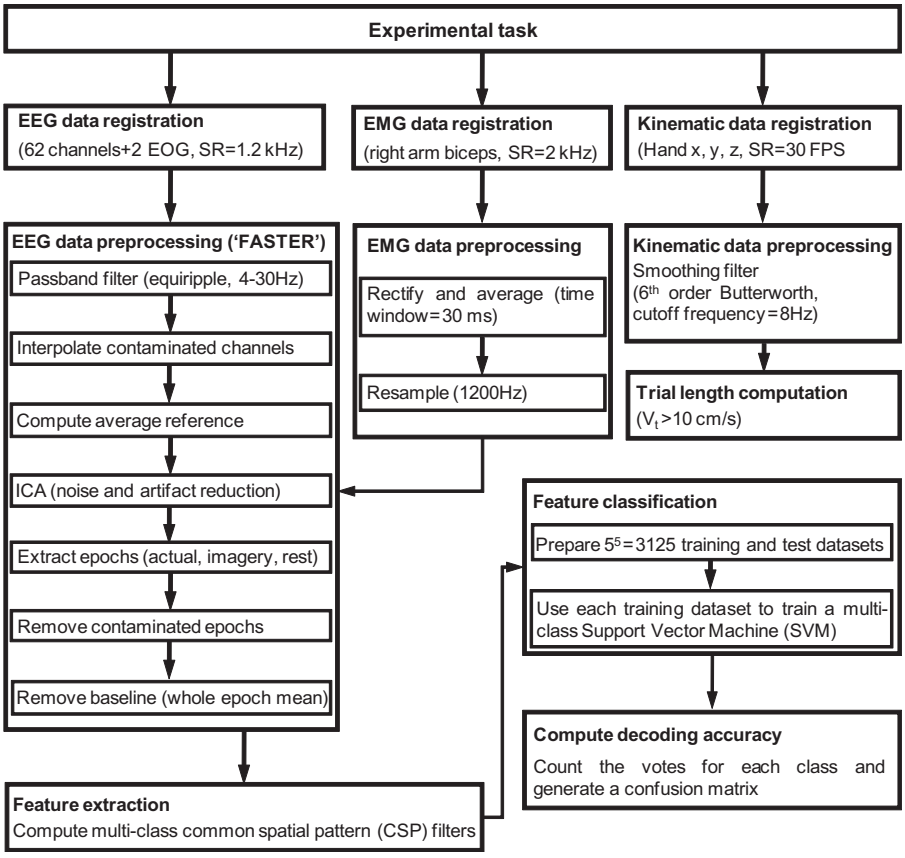

Fig. 2. Preprocessing steps. The flowchart describes the preprocessing steps of the kinematic data and physiological data (both EEG and EMG) and decoding steps, including feature extraction, feature classification and computation of decoding accuracy.

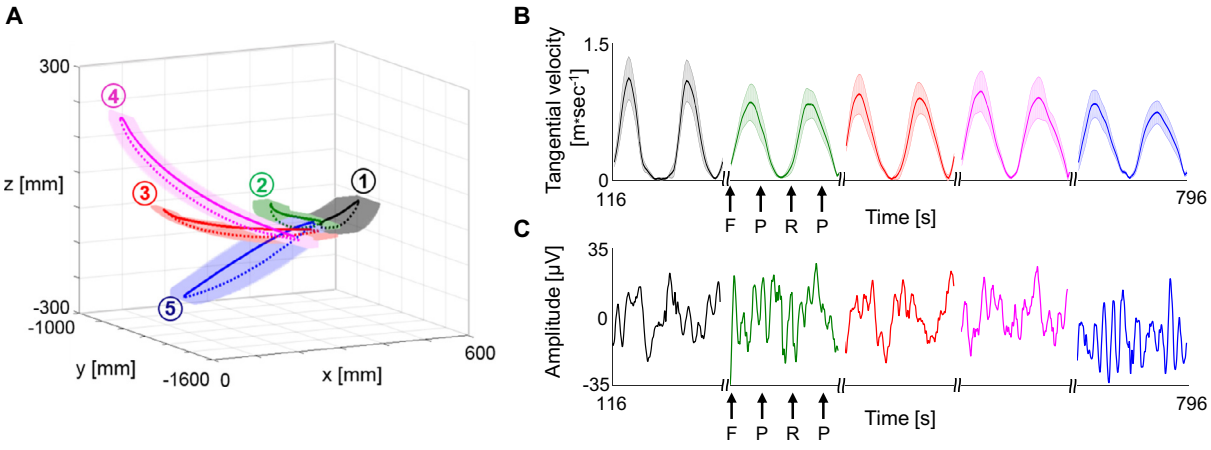

Fig. 3. The subjects generated stereotypical straight point-to-point trajectories with bell-shaped velocity profiles. (A) Mean (SD) path to each target during fast actual movements (FAMs) of a representative subject (#1). (B) Mean (SD) tangential velocity to each target. The arrows indicate the timing of a trigger cue for forward (F), pause (P) and backward (B) movement. (C) Mean EEG waveform of FC3h electrode, positioned over the left sensorimotor area, to each target. The subject generated roughly straight point-to-point trajectories with bell-shaped velocity profile. The corresponding EEG signal was clean of non-physiological and physiological artifacts.

combinations (3125) of training and testing datasets were prepared and tested.

Group II. Each of the five classes data (SAMs to one of the five targets) were divided into five parts, using for each test different 80% of the data to train the decoder and 20% for testing, covering all possible combinations. Each of the training datasets was used to train a multi-class SVM with a radial basis function and classify the corresponding testing dataset. Finally, the votes for each class were counted and a confusion matrix computed. The analysis was performed separately for the 'repetitive' and 'non-repetitive' blocks.

A flowchart summarizing the preprocessing and decoding steps is presented in Fig. 2.

Computing chance level

To assess statistical significance of the classification performance, the distribution of chance classification in the case of finite number of test trials should be considered. To that end, we calculated the probability of getting k correct classifications by chance, which is given by:

$$P(K) = C(n,k) \times P^k \times (1-P)^{n-k}$$

wherein $C(n, k)$ is the number of k combinations out of n test trials and P is the probability of classifying a target in each trial ($1/5 = 0.2$).

For the fast sub block (comprising 24 trials) each dataset comprised 100 training trials (20 trials for each target) and $n = 20$ test trials (four trials for each target). For the slow sub blocks (comprising 15 trials) each dataset comprised 60 training trials (12 trials for each target) and $n = 15$ test trials (three trials for each target). Thus, for example, the chance of the model to accurately decode 35% of the fast trials (e.g., seven trials out of 20) is about 5% and it falls below 0.01% for 60% decoding accuracy.

RESULTS

Group I

First, we visually inspected the EMG and kinematic data to verify that the arm was moving vs. idle during actual movements and imagery trials, respectively, that subjects generated stereotypical point-to-point trajectories to each of the five targets and that the preprocessed EEG data were clean of non-physiological and physiological artifacts (Fig. 3). Next, we tested for movement time differences across targets. No significant difference between movement times (forward and backward) was found across the five targets for each of the subjects for both the slow ($n = 30$, $p > 0.07$, $F < 2.4$) and fast ($n = 48$, $p > 0.07$, $F < 2.3$) actual movements (one-way analysis of variance (ANOVA)). Finally, we tested for a correlation between EOG and kinematics (tangential velocity). The coefficient of determination between the two descriptors was very low ($r^2 < 0.04$) for all subjects (mean ± SD = 0.02 ± 0.02, median = 0.02).

First five blocks – the model estimated the target location with high accuracy. In order to test the model accuracy for decoding target location, the model was trained and tested on a five-class training and testing dataset, respectively. The analysis was performed separately for the two trial types (actual/imagery) and motion speeds (slow/fast). Next, a confusion matrix for each of the four datasets and six subjects was computed (see Experimental procedures). Averaging across subjects, the decoder accuracy for the trained target was significantly higher than chance level for all the four combinations of trial type and speed (84 ± 15%, 84 ± 17%, 77 ± 25% and 79 ± 21% for slow actual, slow imagery, fast actual and fast imagery of movements, respectively; $p < 0.001$) (Table 1). The average target decoding accuracy for both the 'Pause at Home' and 'Pause at Target' epoch was 67 ± 27%, suggesting that both of the rest periods included discriminative neural patterns, probably due to ongoing movement planning processes. Finally, in order to test the model accuracy for decoding target location, irrespective of trial type, all the data were pooled across all conditions for each subject and used to train and test the model. Averaging across subjects, the decoding rate reached 75 ± 22 (72 ± 30%, 74 ± 39%, 77 ± 11%, 62 ± 15%, 81 ± 15 and 84 ± 15 for subject 1–6, respectively). Overall, these findings indicate that neural features during both response (actual or imagined) and rest epochs can be used to decode target location.

First five blocks – the model generalized to different trial types. To study whether decoding a target location is dependent on trial type (actual/imagery) and motion speed (slow/rapid), the model was trained on SAMs to one of the targets and was tested on ISMs to the *same* target, i.e., testing data preceded training data by one sub block (48 s). Averaging across subjects, the model decoded target location with 61 ± 11% accuracy, which is significantly higher than chance level ($p < 0.001$). Decoding rate was also significantly higher than chance level when the training data were exchanged with the testing data, i.e., the model was trained on ISMs and tested on SAMs to the same target (57 ± 19%) or the model was trained on FAMs and tested on IFMs to the same target (63 ± 16%), and vice versa (64 ± 14%) ($p < 0.001$ for all three tests). Overall, these findings indicate that the model generalized well to different trial types (actual/imagery) than those used for training.

In order to test whether the model generalizes to different motion speeds, it was trained on one movement speed and tested on the other one, keeping trial type unchanged, hence, testing data preceded or lagged training data by two sub blocks (96 s). For the actual movements (training on SAMs and testing on FAMs, and vice versa) decoding accuracy was very low (20 ± 7% and 20 ± 2%, respectively) and not significantly different than chance level ($p > 0.2$). Similar results were found for imagery movements, i.e., training on ISMs and testing on IFMs, and vice versa (19 ± 9% and 21 ± 2%, respectively; $p > 0.2$). The model also failed to decode target location when it was

Table 1. The model estimated the target location with high accuracy. A confusion matrix was computed for each trial type, motion speed and pause epoch. Each confusion matrix presents the voting of the model for different targets (rounded percent value), averaged across the six subjects. The target location was correctly estimated (bolded numbers) in 84 ± 15%, 84 ± 17%, 77 ± 25% and 79 ± 21% of the trials for slow actual, slow imagery, fast actual and fast imagery trials, respectively. Target location during 'Pause at Home' and 'Pause at Target' epochs was correctly estimated in 67 ± 27% of the trials, indicating that these epochs comprised target discriminative features

	Slow actual movements						Imagery of slow movements				
Original location	**1**	**96 ± 5**	3 ± 5	0 ± 0	1 ± 1	0 ± 0	**95 ± 7**	4 ± 6	0 ± 1	0 ± 0	0 ± 0
	2	9 ± 10	**82 ± 15**	4 ± 7	4 ± 6	0 ± 0	11 ± 18	**80 ± 19**	7 ± 11	2 ± 4	0 ± 1
	3	0 ± 1	9 ± 9	**79 ± 19**	8 ± 11	3 ± 7	2 ± 4	6 ± 7	**77 ± 16**	7 ± 6	9 ± 12
	4	1 ± 3	4 ± 5	11 ± 10	**73 ± 16**	11 ± 11	1 ± 1	0 ± 1	10 ± 13	**78 ± 24**	11 ± 12
	5	0 ± 0	0 ± 0	3 ± 5	8 ± 10	**88 ± 12**	0 ± 0	1 ± 2	7 ± 9	4 ± 6	**87 ± 14**
	Fast actual movements						Imagery of Fast Movements				
Original location	**1**	**92 ± 9**	5 ± 8	0 ± 0	3 ± 7	0 ± 0	**83 ± 11**	7 ± 5	3 ± 4	6 ± 9	1 ± 2
	2	10 ± 10	**76 ± 19**	12 ± 14	1 ± 3	0 ± 0	10 ± 9	**83 ± 13**	4 ± 6	2 ± 3	0 ± 0
	3	1 ± 2	13 ± 15	**68 ± 29**	14 ± 17	5 ± 11	5 ± 10	5 ± 8	**74 ± 24**	10 ± 9	6 ± 7
	4	3 ± 6	1 ± 1	9 ± 8	**73 ± 30**	14 ± 26	4 ± 5	3 ± 7	16 ± 21	**67 ± 32**	10 ± 14
	5	1 ± 1	0 ± 0	7 ± 9	14 ± 26	**78 ± 32**	2 ± 3	0 ± 0	6 ± 8	5 ± 9	**87 ± 17**
	Pause at Home						Pause at Target				
Original location	**1**	**80 ± 17**	9 ± 10	3 ± 3	8 ± 13	0 ± 1	**79 ± 18**	10 ± 11	3 ± 6	7 ± 12	0 ± 0
	2	12 ± 7	**69 ± 17**	12 ± 16	7 ± 9	0 ± 1	15 ± 13	**67 ± 17**	12 ± 14	5 ± 7	1 ± 1
	3	4 ± 9	16 ± 15	**56 ± 34**	15 ± 16	8 ± 11	5 ± 8	17 ± 16	**54 ± 34**	17 ± 19	8 ± 13
	4	2 ± 3	5 ± 7	18 ± 16	**54 ± 38**	20 ± 24	5 ± 6	4 ± 6	17 ± 19	**53 ± 38**	22 ± 25
	5	0 ± 1	2 ± 4	8 ± 9	12 ± 13	**77 ± 22**	1 ± 1	1 ± 1	7 ± 6	9 ± 9	**83 ± 14**
		1	**2**	**3**	**4**	**5**	**1**	**2**	**3**	**4**	**5**
		Estimated location					Estimated location				

trained on SAMs and tested on IFMs (19 ± 5%, $p > 0.2$) or vice versa, (20 ± 2%, $p > 0.2$), i.e., testing data preceded or lagged training data by three sub blocks (144 s). Thus, target misclassification was found to increase with increasing number of pointed targets during the inter-sets interval (Fig. 4) – from 18 + 20% for testing within the same training sub block to 80 + 4% for testing three sub blocks after training.

Next, we aimed at testing whether the failure of the model to generalize to different motion speeds resulted solely from lack of time proximity between the training and testing sub blocks. To that end, the model was trained and tested on data that were acquired in consecutive sub blocks albeit during the generation of movements with different speeds; the model was trained on slow imagery of movements to a given target and tested on FAMs to the same target, and vice versa. It was found that, for both tests, the model failed to decode target location at significantly different than chance level (21 ± 11%, $p > 0.2$ and 10 ± 1%, respectively; $p > 0.1$) indicating that the inability to generalize to a different speed was not caused by the lack of time proximity between the training and testing sub blocks.

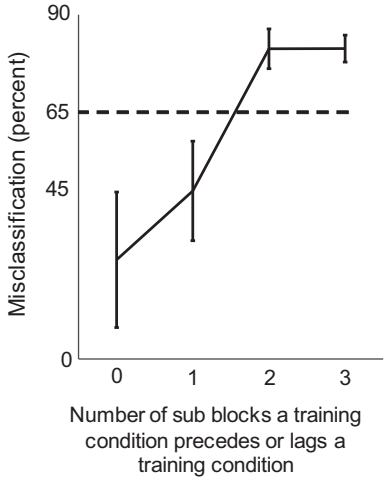

Fig. 4. Target misclassification was positively correlated with the absolute number of sub blocks a training condition precedes or lags a test condition. Dashed line – chance level of target misclassification. The misclassification of a target was below chance level when the trained and tested trials were taken from the same sub block or from consecutive sub blocks.

Last four blocks – decoding accuracy is dependent on target-specific and non-specific mechanisms. Time proximity between a training sub block and a testing sub block, both comprising pointing movements to the same target, may result in enhanced decoding accuracy by two mechanisms: (a) existence of similar baseline brain states (target non-specific), (b) existence of a target-specific, short-term motor memory. In order to dissociate between the effect that two mechanisms may have on decoding accuracy, the subjects practiced a sub block of FAMs to a given target (training data) that was immediately followed by a sub block of IFMs to a *different* target (testing data), thus, the baseline brain state of both sub blocks was kept similar whereas the motor memory was incongruent (see Experimental procedures). The model was trained and tested only on fast movements (actual and imagery) as decoding accuracy was previously found to depend on motion speed.

It was found that when IFMs to a given target followed actual movements to the same target by three sub blocks,

the vote of the model for that target was greatest and significantly higher than chance level (55 ± 5%, 63 ± 16% and 64 ± 7%, respectively; $p < 0.01$ for all tests) and also significantly higher than the vote for the target lastly visited ($p < 0.01$ for all tests), suggesting that short-term, target-specific kinesthetic memory has an enhancing effect on decoding accuracy. However, it was found that when IFMs to a given target followed actual movements to the same target by 10 sub blocks, the model did not vote for that target (i.e., 0%) and the vote was greater for the target lastly visited (70 ± 7%), suggesting that time proximity has a major effect on decoding accuracy.

Group II – movement repetition enhances decoding accuracy

To test whether the high decoding rate was tied with the generation of repetitive movements (block design) to each of the targets, we asked nine naïve subjects to generate both repetitive and non-repetitive, randomized pointing movements to each of the targets. Averaging across subjects, the decoder accuracy for the trained target was significantly higher than chance level when the target was aimed at repeatedly (48 ± 18%, $p = 0.01$). When a sequence of movements, one for each target, was generated repeatedly, the decoding rate of target position was low (30 ± 19%) and not significantly different than chance level ($p > 0.1$) (Table 2). These findings suggest that block design enhances decoding accuracy by time proximity between consecutive trials, possibly due to similar brain state conditions and the consolidation of target-specific motor memory.

Discriminative features are mostly extracted from electrodes positioned over motor areas

In order to detect the electrodes which activity mostly changed across conditions (targets) and thus are preferentially used by the model for discriminating between the five targets, we generated a 2-D topoplot map of the most important (first) CSP filter for each of the six subjects practicing the block design task, trial type (actual or imagery), motion speed (slow or fast) and pause epoch (pause-at-home or pause-at-target). The contribution of each electrode corresponds to its absolute weight averaged across the different training and testing datasets. Next, we generated a topoplot for each of the two trial types, motion speed and pause epochs, averaged across subjects. The six topoplots exhibited a similar topography pattern wherein the most discriminative features were extracted from electrodes positioned over the contralateral sensorimotor area (electrode C3h), the ipsilateral prefrontal cortex (electrode F2) and the ipsilateral sensorimotor or somatosensory cortex (electrode CCP4h) (Fig. 5). These findings suggest that for all actual and imagery movements or resting epochs, decoding of target location relied mostly on changes in the spectro-temporal activation pattern in these electrodes rather than on a change in the spatial activation pattern.

DISCUSSION

Given the relatively low spatial resolution of the EEG signals, the discrimination of neural activity patterns between actual or imagined pointing movements to targets in 3D space has to rely heavily on spectro-temporal rather than spatial differences. We suggest that the segregation of the neural representation of target locations could be enhanced by forming a strong recollection of each of the response (motor memory), which is known to be induced when an action is generated repeatedly (Krakauer and Shadmehr, 2006). To that end, we devised a block design task wherein an actual or imagined movement to a target was repeated consecutively for several times (Fig. 1). The response type (actual/imagery, slow/fast) and order of the sub blocks within the first five blocks were set to test the specificity and generality of the devised classification model.

The EEG data were passband filtered in 4–30 Hz. Although signal features for decoding the direction of movement and kinematics in 3D reach-to-grasp task are most often extracted from the lowest frequency band (i.e., delta) (Agashe and Contreras-Vidal, 2011; Brinkman et al., 2014; Paek et al., 2014; Agashe et al., 2015), we used only the mid-range frequencies (i.e., theta, mu, alpha and beta) in order to attenuate potential low-frequency (e.g., drift, arm movement) and high-frequency (e.g., EMG) artifacts and ensure that the decoding of target location resulted from distinct neural patterns, rather than non-neural sources. Moreover, EOG, EMG and movement artifacts were later removed by ICA. Overall, the model decoded actual movements (slow and fast) with 80% accuracy (Table 1), which is

Table 2. Repetitive movements to the same target enhanced decoding of target location. A confusion matrix was computed for both the repetitive and non-repetitive (randomized) trials for the Group II. The decoding accuracy (rounded percent value) averaged across subjects for the non-repetitive trials was very low (30 ± 19%) and not significantly different than chance level ($p > 0.1$). The average decoding accuracy for the repetitive trials was significantly higher than chance level (48 ± 18%, $p = 0.01$)

		Repetitive movements					Non-repetitive movements				
Original location	**1**	**42 ± 17**	27 ± 14	10 ± 8	10 ± 5	10 ± 9	**36 ± 22**	15 ± 3	22 ± 13	16 ± 7	12 ± 6
	2	25 ± 7	**36 ± 19**	13 ± 15	13 ± 8	13 ± 10	21 ± 7	**21 ± 14**	18 ± 4	19 ± 8	21 ± 10
	3	7 ± 5	8 ± 5	**56 ± 15**	12 ± 7	18 ± 10	23 ± 8	15 ± 3	**22 ± 11**	20 ± 6	19 ± 4
	4	8 ± 4	11 ± 7	14 ± 7	**47 ± 15**	21 ± 7	12 ± 6	14 ± 8	16 ± 7	**42 ± 23**	16 ± 7
	5	8 ± 8	5 ± 4	14 ± 6	11 ± 6	**61 ± 17**	12 ± 4	19 ± 9	18 ± 5	21 ± 7	**30 ± 19**
		1	**2**	**3**	**4**	**5**	**1**	**2**	**3**	**4**	**5**
		Estimated location					Estimated location				

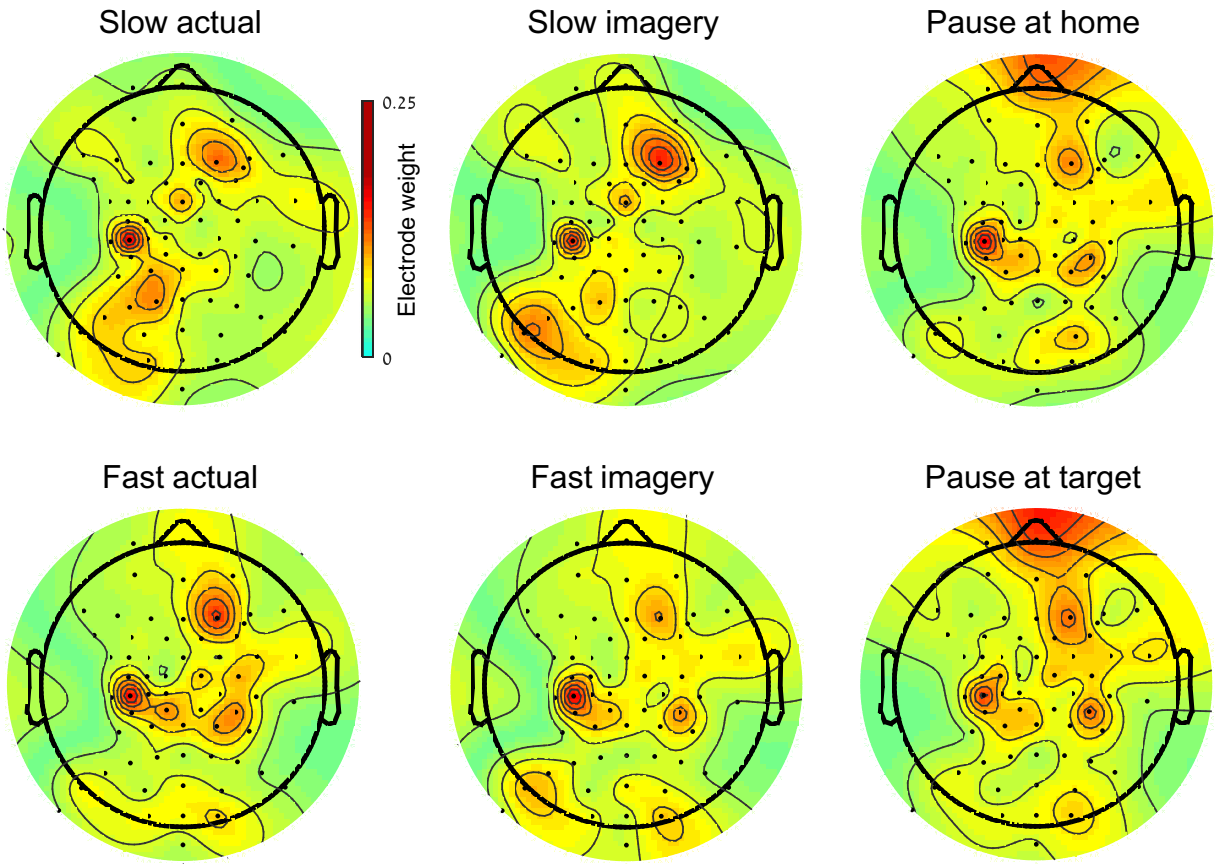

Fig. 5. Electrodes positioned over motor areas conveyed most of the discriminative neural features. Depicted are 2-D topoplots, averaged across the six subjects, of the most important CSP filter (i.e., explaining the largest variance of activation between the five targets) for each movement trial (actual or imagery, slow or fast) and rest period (Pause at Home and Pause at Target). Color bar – electrode weight. The electrodes who conveyed most of the discriminative features across targets were positioned above the contralateral primary motor area, ipsilateral intermediate frontal gyrus and ipsilateral somatosensory association cortex.

much higher than chance level (20%) and corresponds to a kappa coefficient of 75. The high decoding rate was not caused by difference in reach time to different targets as analysis of movement time data showed that it was not significantly different across the five targets. The classifier was also successful in decoding imagery movements (slow and fast), reaching 81% accuracy. To the best of our knowledge, no work has reported achieving this high a decoding rate of imagined movements taking into account the high number of targets (classes). The high decoding rate is remarkable as all the pointing movements were generated with the same limb and aimed at relatively adjacent targets in the 3D space, hence, the same motor-related areas were activated across all conditions. The model generalized well for different trial types; the average decoding accuracy was 61% when training was performed using slow or FAMs and testing was done on imagery of slow or fast movement, respectively, and vice versa. These findings are encouraging as an efficient brain–computer interface (BCI) system for disabled subjects should have the ability to decode imagined movements with high accuracy rate.

The high decoding rate of target position was tied to the use of a block design, i.e., time proximity between adjacent training or testing trials; analyzing the decoding rate of Group II has shown that the model classified the targets correctly 48% of the trials when subjects generated repetitive (block) pointing movements and was not significantly different than chance level, when the subjects practiced sequences of pointing movements to different targets (Table 2). Moreover, cross validation (generalization) analyses performed on the first five blocks of Group I have shown that target misclassification increased with increased number of intervening sub blocks and elapsed time between the trained and tested conditions (Fig. 4). Finally, the analysis performed on the data that were registered in the last four blocks of Group I revealed that an imagined movement to a given target was mainly decoded as an actual movement to the target that was lastly visited, irrespective of its location, indicating that time proximity has indeed a major impact on decoding performance. As EEG signals are inherently non-stationary (Nunez, 2000), testing a model on data that were acquired proximately in time to training data may result in enhanced decoding accuracy simply due to similar brain states or environmental conditions. These brain states presumably manifest different levels of fatigue, attention or motivation throughout practice rather than common signal artifacts such as baseline drifts as these were removed.

Several observations indicate that time proximity between consecutive trials may lead to enhanced decoding accuracy by an additional short-term mechanism which is *target-specific* and is manifested by distinct neural patterns: (a) The voting of the classifier for a target that was aimed at several blocks before increase if that target matched the tested target (compared to an unmatched target that was trained the *same* number of blocks before); (b) The decoding accuracy was higher if the trained and tested target were aimed at with the same speed (fast or slow), compared to different aiming speeds, despite the longer time interval between the two conditions (two sub blocks vs. one sub block), which are more likely to result in changes of brain state conditions and, thus, reduced decoding accuracy; (c) Target decoding during the pause epochs (both 'pause-at-home' and 'pause-at-target') preceding the pointing movements was significantly higher than chance level, albeit lower than the decoding rate of the imagined movements (slow and fast). As both the hand and eyes were idle during the pause epochs, the decoding could be attributed to target non-specific mechanisms (different brain states) and/or target-specific mechanisms (planning processes preceding each pointing movement).

An additional indication of the contribution of a target-specific mechanism to the high decoding rate is the similar spatial pattern of neural activation across conditions; had time proximity between training and testing epochs led to high decoding accuracy solely due to similar environmental conditions, different electrodes could presumably provide the most discriminative features for different conditions as different brain areas may change activity differently with time. However, a similar set of electrodes was found to provide the most discriminative neural features for each of the four conditions and two rest epochs (Fig. 5). Moreover, these electrodes were positioned mainly over motor related areas – the contralateral sensorimotor cortex, the ipsilateral prefrontal cortex and somatosensory cortex, long-known to be engaged in motor learning, motor imagery and visuomotor coordination (Georgopoulos et al., 1986; Decety et al., 1994; Scott and Kalaska, 1995; Kakei et al., 1999; Moran and Schwartz, 1999). Overall, these findings suggest that even if the successful decoding of the pause epochs resulted solely from target non-specific mechanism, the significantly higher decoding rate of the imagined movements, for which the hand and eyes were idle, is most likely linked to target-specific neural mechanisms.

The decoding accuracy of the repetitive blocks of SAM of Group II (48%, Table 2) were much lower than that of the SAM blocks of Group I (84%, Table 1). This finding suggests the lack of imagery trials for Group II may have led to a less discriminable neural representation of target position.

Previous behavioral and neurophysiological studies have suggested that the acquisition and retention of motor skills may result in significant experience-related reorganization within specific motor cortical representations in the adult human brain (Karni et al., 1995; Mandelblat-Cerf et al., 2011) and that even limited training experience (several minutes) can be sufficient to trigger performance gains that require time to become evident (Karni et al., 1998). Hence, it may be that generating repetitive movements, albeit brief in time (48 s), to each of the targets induced target- and trial-type-distinct neural patterns that were used by the model and resulted in high decoding rates. It is possible that as the time interval between the training and testing blocks increased, the target-specific motor memory waned, which resulted in greater target misclassification.

Deciphering the mechanisms underlying the enhanced decoding accuracy found for the block design could ultimately be useful in more general settings wherein movements are not executed in blocks. A possible setup for enhancing the decoding of single trial motor imagery may be to vibrate muscle tendon. Tendon muscle vibration was proposed as a new calibrating and task guidance methodology to further improve motor imagery BCI by inducing a pseudo-kinesthetic sensation. It has been suggested that subjects' simulated kinesthetic experience during motor imagery task is enhanced by accessing sensory experiences from the illusory stimulation, which could help make motor imagery more applicable to BCI (Yao et al., 2015). Assuming that muscle tendon vibration leads to the formation of segregated neural patterns it remains to be studied whether cyclic, repetitive vibration of the muscle tendons that are typically involved in the generation of different pointing movements will enhance the decoding of single trial motor imagery. This will substitute the need for a block design and enable the devise of an efficient EEG-based BCI that can be used to control robotic assistive devices to improve upper-extremity motor recovery in individuals with stroke.

Open questions

The findings of the current study raise several questions. First, the confusion matrices computed for Group I (Table 1) and Group II (Table 2) showed that the model decoded target location with high accuracy. Examining the off diagonal values reveals that the voting for any given target decreased as it got further away in time (and number of blocks) from the tested target. As was previously suggested, time proximity between trained and tested conditions may affect decoding performance both by target-specific and non-specific mechanisms. However, decoding performance may also depend on the spatial proximity and/or the relative position of the trained target with respect to the tested target. Future studies will need to carefully control and test for the possible effect of time and spatial proximity between the trained and tested targets on decoding accuracy. Second, repeating pointing movements for a short time period of 48 s was sufficient to induce segregation in the neural patterns, which was used by the model to decode target location with high accuracy. It remains to be studied the nature of the spectrotemporal changes in

the neural patterns and the dependency of decoding performance on trial length, rest period and number of trials in a sub block. Finally, the effect of target-specific mechanisms on decoding performance was shown to diminish as the time interval between the trained and tested sub blocks increased. However, increasing the time interval correlated with an increased number of different targets that were pointed at during that time period. Hence, the waning of target-specific motor memory may have also resulted from motor memory interference. Future works will study the effect of time and motor memory interference on decoding accuracy of target location.

CONCLUSION

Overall, our findings suggest that block design enhances the decoding accuracy of target location and that the high decoding rate is generalized to different trial types. Deciphering the mechanisms underlying the enhanced decoding accuracy found for the block design and the effect of motor memory on decoding performance can ultimately be used in more general settings wherein movements are not executed in blocks.

Acknowledgments—This research was supported by the Israel Science Foundation (grant No. 76/12) and, in part, by Merit Review Award CX-0004-37 from the U.S. Department of Veterans Affairs Clinical Sciences Research and Development Program.

The authors declare no competing financial interests.

REFERENCES

Agashe HA, Contreras-Vidal JL (2011) Reconstructing hand kinematics during reach to grasp movements from electroencephalographic signals. In: 33th annual international conference of the IEEE Engineering in Medicine and Biology Society (EMBC) (Boston, USA).

Agashe HA, Paek AY, Zhang Y, Contreras-Vidal JL (2015) Global cortical activity predicts shape of hand during grasping. Front Neurosci 9:121.

Antelis JM, Montesano L, Minguez J (2011) Towards decoding 3D finger trajectories from EEG. Int J Bioelectromagnetism 13 (3):112–114.

Bai O, Rathi V, Lin P, Huang D, Battapady H, Fei D, Schneider L, Houdayer E, Chen X, Hallett M (2011) Prediction of human voluntary movement before it occurs. Clin Neurophysiol 122:364–372.

Bradberry TJ, Gentili RJ, Contreras-Vidal JL (2010) Reconstructing three-dimensional hand movements from noninvasive electroencephalographic signals. J Neurosci 30(9):3432–3437.

Brashers-Krug T, Shadmehr R, Bizzi E (1996) Consolidation in human motor memory. Nature:382.

Brinkman L, Stolk A, Dijkerman H, de Lange F, Toni I (2014) Distinct roles for alpha- and beta-band oscillations during mental simulation of goal-directed actions. J Neurosci 34:14783–14792.

Crammer K, Singer Y (2001) On the algorithmic implementation of multi-class SVM. JMLR 2:265–292.

Decety J, Perani D, Jeannerod M, Bettinardi V, Tadary B, Woods R, Mazziotta JC, Fazio F (1994) Mapping motor representations with positron emission tomography. Nature 371(6498):600–602.

Deecke L, Kornhuber H (2003) Human freedom, reasoned will, and the brain. The Bereitschaftspotential story. In: Jahanshahi M, Hallett M, editors. The Bereitschaftspotential, movement-related cortical potentials. Kluwer Academic/Plenum. p. 283–320.

Delorme A, Makeig S (2004) EEGLAB: an open source toolbox for analysis of single-trial EEG dynamics. J Neurosci Methods 134:9–21.

Georgopoulos AP, Schwartz AB, Kettner RE (1986) Neuronal population coding of movement direction. Science 233 (4771):1416–1419.

Grosse-Wentrup M, Buss M (2008) Multiclass common spatial patterns and information theoretic feature extraction. IEEE Trans Biomed Eng 55(8):1991–2000.

Hammon P, Makeig S, Poizner H, Todorov E, de Sa V (2008) Predicting reaching targets from human EEG. IEEE Signal Process Mag 25:69–77.

Huang D, Lin P, Fei D, Chen X, Bai O (2009) Decoding human motor activity from EEG single trials for a discrete two-dimensional cursor control. J Neural Eng 6:046005.

Kakei S, Hoffman D, Strick P (1999) Muscle and movement representations in the primary motor cortex. Science 285 (5436):2136–2139.

Karni A, Meyer G, Jezzard P, Adams M, Turner R, Ungerleider L (1995) Functional MRI evidence for adult motor cortex plasticity during motor skill learning. Nature 377:155–158.

Karni A, Meyer G, Rey-Hipolito C, Jezzard P, Adams M, Turner R, Ungerleider L (1998) The acquisition of skilled motor performance: fast and slow experience-driven changes in primary motor cortex. Proc Natl Acad Sci USA 95:861–868.

Kilner J, Vargas C, Duval S, Blakemore S, Sirigu A (2004) Motor activation prior to observation of a predicted movement. Nat Neurosci 7:1299–1301.

Krakauer J, Shadmehr R (2006) Consolidation of motor memory. Trends Neurosci 29:58–64.

Lakany H, Conway B (2007) Understanding intention of movement from electroencephalograms. Expert Syst 24:295–304.

Lew E, Chavarriaga R, Silvoni S, Millan Jdel R (2014) Single trial prediction of self-paced reaching directions from EEG signals. Front Neurosci 8:222.

Mandelblat-Cerf Y, Novick I, Paz R, Link Y, Freeman S, Vaadia E (2011) The neuronal basis of long-term sensorimotor learning. J Neurosci 31:300–313.

Moran DW, Schwartz AB (1999) Motor cortical representation of speed and direction during reaching. J Neurophysiol 82 (5):2676–2692.

Nam C, Jeon Y, Kim Y, Lee I, Park K (2011) Movement imagery-related lateralization of event-related (de)synchronization (ERD/ERS): motor-imagery duration effects. Clin Neurophysiol 122:567–577.

Niazi I, Jiang N, Tiberghien O, Nielsen J, Dremstrup K, Farina D (2011) Detection of movement intention from single-trial movement-related cortical potentials. J Neural Eng 8:066009.

Nolan H, Whelan R, Reilly RB (2010) FASTER: fully automated statistical thresholding for EEG artifact rejection. J Neurosci Methods 192:152–162.

Nunez P (2000) Toward a quantitative description of large-scale neocortical dynamic function and EEG. Behav Brain Sci 23:371–437.

Ofner P, Muller-Putz G (2015) Using a noninvasive decoding method to classify rhythmic movement imaginations of the arm in two planes. IEEE Trans Biomed Eng 62:972–981.

Paek AY, Agashe HA, Contreras-Vidal JL (2014) Decoding repetitive finger movements with brain activity acquired via non-invasive electroencephalography. Front Neuroeng 7:3.

Pfurtscheller G, Brunner C, Schlögl A, Lopes da Silva F (2006) Mu rhythm (de)synchronization and EEG single-trial classification of different motor imagery tasks. NeuroImage 311:53–159.

Rickert J, de Oliveira S, Vaadia E, Aertsen A, Rotter S, Mehring C (2005) Encoding of movement direction in different frequency ranges of motor cortical local field potentials. J Neurosci 25:8815–8824.

Robinson N, Guan C, Vinod A, Ang K, Tee K (2013) Multi-class EEG classification of voluntary hand movement directions. J Neural Eng 10:056018.

Scherer R, Muller G, Neuper C, Graimann B, Pfurtscheller G (2004) An asynchronously controlled EEG-based virtual keyboard: improvement of the spelling rate. IEEE Trans Biomed Eng 51:979–1307.

Scott SH, Kalaska JF (1995) Changes in motor cortex activity during reaching movements with similar hand paths but different arm postures. J Neurophysiol 73(6):2563–2567.

Shadmehr R, Holcomb HH (1997) Neural correlates of motor memory consolidation. Science 227:821–825.

Tzagarakis C, Ince NF, Leuthold AC, Pellizzer G (2010) Beta-band activity during motor planning reflects response uncertainty. J Neurosci 3011:270–11277.

Waldert S, Preissl H, Demandt E, Braun C, Birbaumer N, Aertsen A, Mehring C (2008) Hand movement direction decoded from MEG and EEG. J Neurosci 28:1000–1008.

Wolpaw J, McFarland D (2004) Control of a two-dimensional movement signal by a non-invasive brain-computer interface in humans. Proc Natl Acad Sci USA 1011:7849–17854.

Yao L, Meng J, Sheng X, Zhang D, Zhu X (2015) A novel calibration and task guidance framework for motor imagery BCI via a tendon vibration induced sensation with kinesthesia illusion. J Neural Eng 12(1):016005.

(Accepted 10 May 2016)
(Available online 17 May 2016)